Composition-driven phase coexistence and functional properties of the (1-x)BZT-(x)BCT ceramics near the phase convergence region

Jirapa TANGSRITRAKUL[1,2,*], Chumpon WICHITTANAKOM[3], and Chatree SAIYASOMBAT[4]

[1] *Department of Materials and Textile Technology, Faculty of Science and Technology, Thammasat University, Pathum Thani, 12120, Thailand*
[2] *Thammasat University Research Unit in Sustainable Materials and Circular Economy, Thammasat University, Pathum Thani, 12120, Thailand*
[3] *Department of Physics, Faculty of Science and Technology, Thammasat University, Pathum Thani, 12120, Thailand*
[4] *Synchrotron Light Research Institute, Nakhon Ratchasima, 30000, Thailand*

*Corresponding author e-mail: tjirapa@tu.ac.th

Abstract

The concept of composition-induced phase transformation in Lead Zirconate Titanate (PZT) at the Morphotropic Phase Boundary (MPB) has been employed to improve functional properties of the (1-x)BZT-(x)BCT ceramic. However, it was observed that the phase diagram of the (1-x)BZT-(x)BCT ceramic is different to the PZT. As a result, the nature of the superior functional properties found in (1-x)BZT-(x)BCT ceramic is unlike PZT and still unclear so far. In this work, functional properties; dielectric, ferroelectric, energy storage, and piezoelectric properties, of the (1-x)BZT-(x)BCT ceramics where x = 0.3 mol% to 0.6 mol% were evaluated at room temperature in comparison to the identification of phase coexistence using synchrotron x-ray powder diffraction (SXPD). This work found that changes of BCT content had a strong impact on the observed coexisting phases and functional properties. Moreover, the composition that showed the highest piezoelectric properties did not present the largest of saturation polarization. This implies that the functional properties of the (1-x)BZT-(x)BCT ceramics are not dependent on the presence of polarizations under the application of electric field. The contribution of non-180° domain switching also plays a vital role, especially in the piezoelectric properties. These findings would help to extend our knowledge of the nature of the (1-x)BZT-(x)BCT ceramic.

1. Introduction

Electroceramics, such as Lead Zirconate Titanate (PZT) or Barium Titanate ($BaTiO_3$), have been widely used for many decades as sensors, actuators, dielectric capacitors, etc. [1-6]. However, the restriction of toxic Pb used in electrical and electronic equipment has been triggered by European Union (EU) legislation, resulting in the development of non-toxic materials for PZT replacement [7]. Initially, it is well known that functional properties of $BaTiO_3$-based ceramics are not excellent for practical applications until the discovery of high piezo-electricity in the $Ba(Zr,Ti)O_3$-$(Ba,Ca)TiO_3$ system was reported in 2009 [8]. The concept of composition-induced phase transformation between two crystal structures, as observed in the phase diagram of PZT at the morphotropic phase boundary (MPB), was employed to improve functional properties of the $Ba(Zr,Ti)O_3$-$(Ba,Ca)TiO_3$ ceramic [3,8].

The coexistence of rhombohedral (R) and tetragonal (T) at MPB composition in the phase diagram of the $(1-x)Ba(Ti_{0.8}Zr_{0.2})O_3$-$(x)(Ba_{0.7}Ca_{0.3})TiO_3$ or BZT-xBCT ceramics was first reported by Liu *et al.*, leading to the presence of high piezoelectric coefficient (d_{33}) that comparable to PZT on the BZT-xBCT ceramics [8]. Moreover, the distortion of MPB with the existence of Cubic-Rhombohedral-Tetragonal (C-R-T) triple point was illustrated in the phase diagram of the BZT-xBCT ceramics which contradict to the phase diagram of

PZT [8]. Then, the revised phase diagram of the BZT-xBCT ceramics has been demonstrated since the intermediate orthorhombic (O) phase was observed by Keeble *et al*. [9] In addition, a C-R-T triple point has been suggested to a region called phase convergence region instead due to the Gibbs phase rule [9]. However, the occurrence of multiphase coexisting point (MCP) in the phase diagram is still unclear and requires further investigation [10].

Many studies showed that the superior functional properties often found in the 50BZT-50BCT composition, indicating the MPB composition [8,11-13]. However, the influences of phase boundary and phase convergence region on the functional properties of the BZT-xBCT ceramics are different and requires more research to clarify this point [14]. This work aims to investigate the functional properties of the (1-x)BZT-(x)BCT ceramics as a function of composition near phase convergence region using high-resolution synchrotron XRD to evaluate the coexisting phases.

2. Experimental methods

The $(1-x)Ba(Ti_{0.8}Zr_{0.2})O_3$-$(x)(Ba_{0.7}Ca_{0.3})TiO_3$ or (1-x)BZT-(x) BCT ceramics where x = 0.3 mol% to 0.6 mol%, near phase convergence region (referred as 70BZT-30BCT, 60BZT-40BCT, 50BZT-50BCT, and 40BZT-60BCT, respectively), were prepared via solid-state reaction.

The raw powders of $BaCO_3$ (99.0%), $CaCO_3$ (99.0%), TiO_2 (99.0%) and ZrO_2 (99.0%) were milled for 24 h in ethanol using Yttria-Stabilized Zirconia beads with diameter of 5 mm in 60 mL poly-propylene bottle. Then, the milled powders were dried overnight at 90°C before calcination at 1250°C for 3 h with heating rate of 5°C·min⁻¹. After that, the calcined powders were milled for another 24 h and dried overnight prior to pressing into a disc shape with a diameter of 13 mm and a thickness of 2 mm, approximately. Next, the green bodies were sintered at 1450°C for 3 h with heating rate of 5°C·min⁻¹ in a closed alumina crucible to obtain the (1-x)BZT-(x)BCT ceramics.

Phase coexistence of the (1-x)BZT-(x)BCT ceramics was investigated by synchrotron x-ray powder diffraction (SXPD) with a photon energy of 12 keV (λ = 1.0332 Å) on beamline BL1.1W at Synchrotron Light Research Institute, Thailand. In this work, the SXPD patterns of the (1-x)BZT-(x)BCT ceramics were collected by a Mythen detector from 2θ between 13° and 73° for 400 s The full-pattern refinement was studied by Rietveld method using Topas software (version 5.0, Bruker) to identify the coexisting phases of the (1-x)BZT-(x)BCT ceramics. The crystallographic information files (CIF files) from crystallography open database (COD) were employed for Rietveld refinement [15]. In addition, the surface micro-structure of the (1-x)BZT-(x)BCT ceramics was observed by scanning electron microscope (JEOL, JCM-6000). The average grain size was evaluated via linear intercept method with a proportionality constant (k) of 1.126 [16].

To conduct the electrical measurement, the (1-x)BZT-(x)BCT ceramics were ground into a thickness of ~1 mm using a P800 SiC paper. Next, the silver electrode (Heraeus PCC11889, Germany) was applied on both parallel surfaces of the ceramic disc and then fired at 550°C for 1 h. The LCR meter (Agilent E4980A precision LCR meter) was employed to measure the frequency-dependent dielectric properties

with a frequency range of 10 Hz to 10⁶ Hz. The polarization and strain as a function of electric field (P-E hysteresis loop and s-E butterfly loop, respectively) were conducted by applying bipolar electric field of ± 10 kV·cm⁻¹ to ± 40 kV·cm⁻¹ with a frequency of 2 Hz using the Precision Premier II ferroelectric tester (Radient Technologies, inc.). Energy storage properties were evaluated by numerical integration of the P-E hysteresis loop using the trapezoidal rule.

3. Results and discussion

3.1 Synchrotron x-ray powder diffraction profiles

To fully understand the occurrence of phase coexistence in the (1-x)BZT-(x)BCT ceramics near phase convergence region, the synchrotron x-ray powder diffraction (SXPD) is needed because it has higher resolution in comparison to laboratory XRD and low instrumental contributions to peak broadening [17]. Figure 1(a) illustrates the room-temperature SXPD profiles of the 70BZT-30BCT, 60BZT-40BCT, 50BZT-50BCT, and 40BZT-60BCT ceramics. It was found that all compositions showed pure perovskite structure without trace of secondary phase, indicating that the calcination and sintering temperatures used in this work were appropriate for synthesis of the (1-x)BZT-(x)BCT ceramics. Moreover, changes in peak splitting were clearly observed when BCT content increased, as seen in Figure 1(b). This implies that phase transformation with the multiple coexisting phases may occur in the (1-x)BZT-(x)BCT ceramics. Further analysis of phase identification by full-pattern refinement is shown later in Figure 3. In addition, the substitution of small Ca^{2+} (1.34 Å) into Ba^{2+} (1.61 Å) and large Zr^{4+} (0.86 Å) into Ti^{4+} (0.745 Å) caused a slight drop of lattice spacing, resulting in a gradual shift of SXPD pattern to higher 2θ as BCT content increased [18,19].
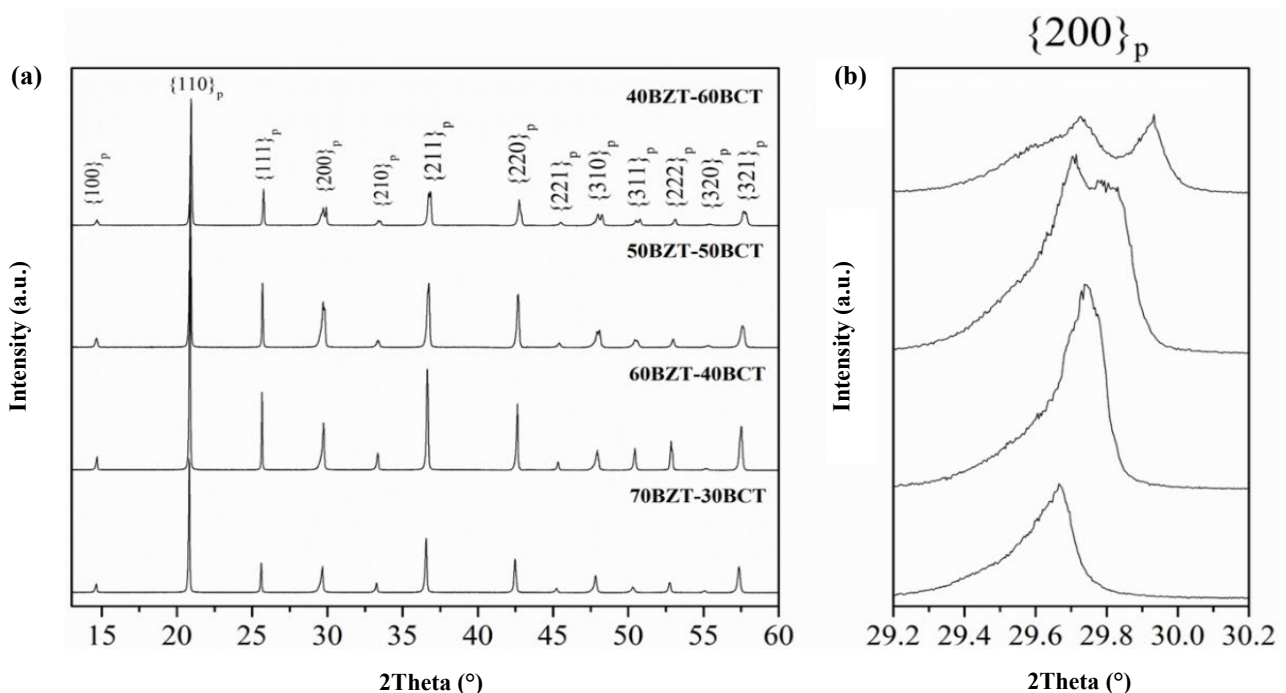
Figure 1. (a) The SXPD patterns of the (1-x)BZT-(x)BCT ceramics and (b) the enlargement of $\{200\}_p$ reflection, showing the evolution of phase transformations with increasing BCT contents. (λ = 1.0332Å).

The coexisting phases of the (1-x)BZT-(x)BCT ceramics were identified by full-pattern refinement, as illustrated in Figure 2. Additionally, the enlargement of pattern refinement for {110}$_P$, {111}$_P$, and {200}$_P$ reflections is presented in Figure 3. Structure models of rhombohedral (R, spacegroup *R3mR*), orthorhombic (O, spacegroup *Amm2*), tetragonal (T, spacegroup *P4mm*), and cubic (C, spacegroup *Pm3m*) were used for fitting. In this work, the best fit for the 70BZT-30BCT ceramic was obtained by fitting with a model of R and C coexisting phases, giving the lowest goodness-of-fit (GOF) of 2.08 with R-phase fraction of 69% and C-phase fraction of 31%. When increasing BCT to 40BCT, it was found that the SXPD profile was best fitted to the coexisting phases of R (70%) and O (30%) with the GOF of 3.74. Moreover, as further increased the amount of BCT, the R-phase disappeared and the O-phase fraction increased to 75% with the occurrence of a small T-phase fraction (25%) for the 50BZT-50BCT ceramic. This implied that these compositions occurred near the R-O and O-T phase boundaries of the (1-x)BZT-(x)BCT phase diagram, respectively. Then, the disappearance of the O phase was observed with the coexistence of 71%T and 29%C phases for the 40BZT-60BCT ceramic. Note that phase fraction and GOF values obtained by full-pattern refinement for all compositions are also summarized in Table 1.
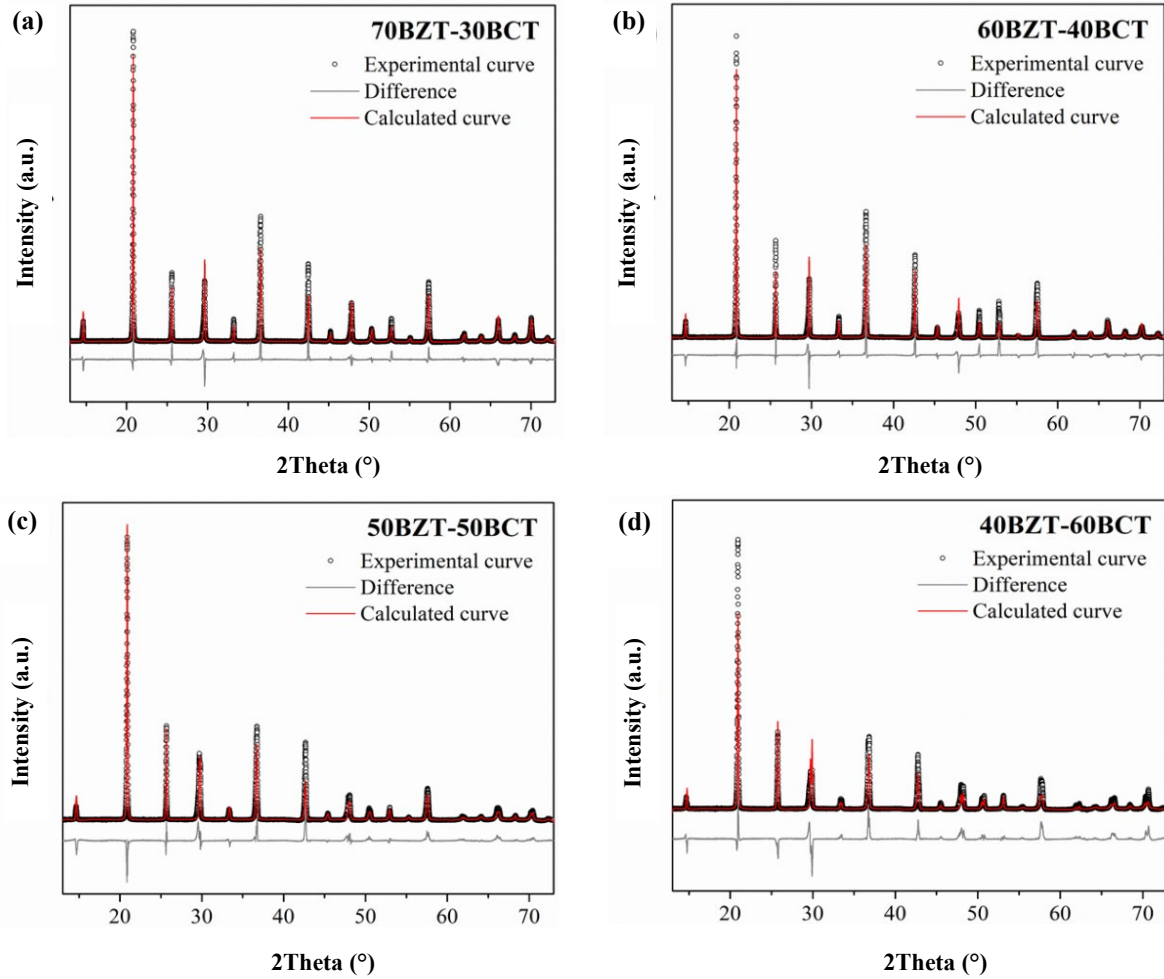
Figure 2. The experimental, calculated, and difference curves obtained by full-pattern refinement of the (a) 70BZT-30BCT, (b) 60BZT-40BCT, (c) 50BZT-50BCT, and (d) 40BZT-60BCT ceramics. (λ = 1.0332Å).

Table 1. Summary of phase fraction, goodness-of-fit (GOF), average grain size, dielectric permittivity (ε_r), loss tangent (tan δ), coercive field (E_c), the difference between P_{sat} and P_r (ΔP), energy conversion efficiency (η), and converse piezoelectric coefficient (d_{33}) for the (1-x)BZT-(x)BCT ceramics near phase convergence region.

Composition	Phase fraction (%)	GOF	Grain size (µm)	ε_r*	tan δ*	E_c** (kV·cm⁻¹)	ΔP** (µC·cm⁻²)	η** (%)	d_{33}** (pm·V⁻¹)
70BZT-30BCT	R=69, C=31	2.08	5 ± 0.9	3214	0.058	1.59	11.50	70.40	178.75
60BZT-40BCT	R=70, O=30	3.74	6.6 ± 1.1	2543	0.058	2.20	10.47	65.32	341.25
50BZT-50BCT	O=75, T=25	3.61	11.1 ± 1.8	2466	0.114	2.92	10.34	60.59	392.5
40BZT-60BCT	T=71, C=29	3.80	8.1 ± 1.5	1809	0.013	6.12	9.20	45.10	292.5

*　　Measured at 10 Hz

**　　Measured at ± 40 kV·cm⁻¹ with frequency of 2 Hz
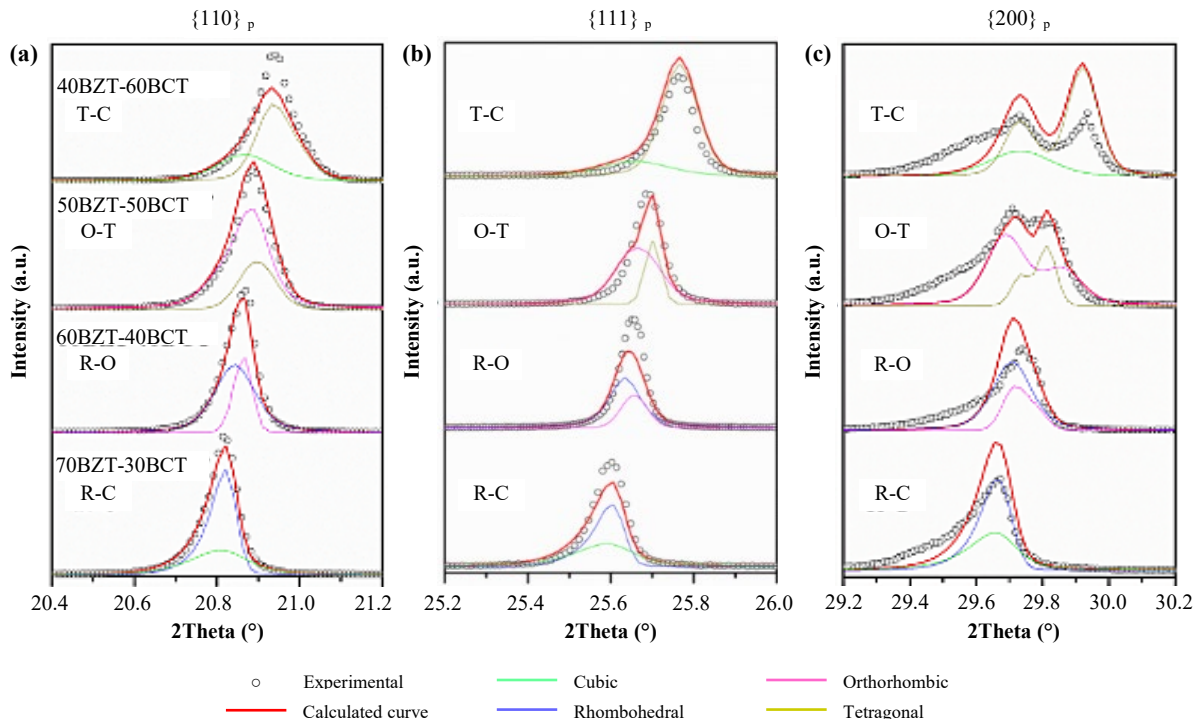
Figure 3. The enlargement of full-pattern refinement for (a) $\{110\}_P$, (b) $\{111\}_P$, and (c) $\{200\}_P$ reflections, showing phase coexistence of R-C, R-O, O-T, and T-C in the 70BZT-30BCT, 60BZT-40BCT, 50BZT-50BCT, and 40BZT-60BCT ceramics, respectively. ($\lambda = 1.0332$Å).
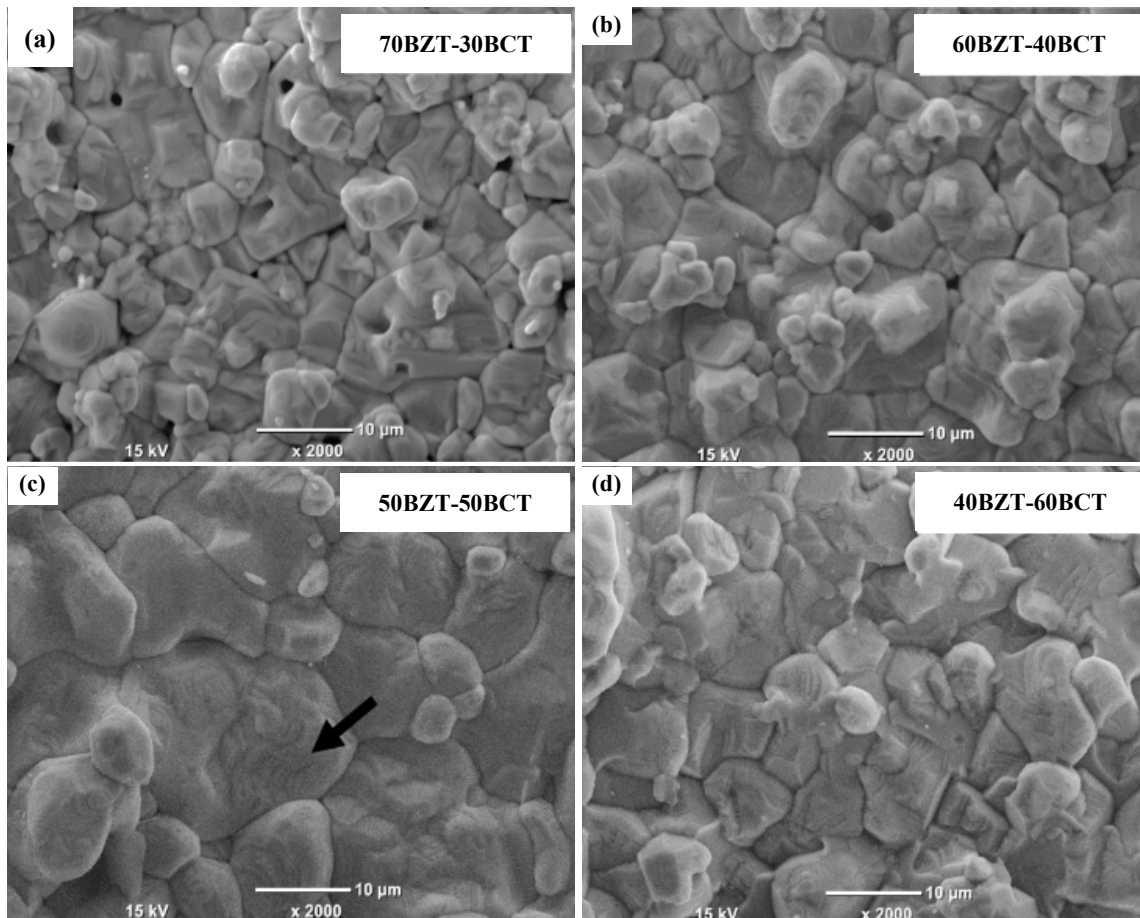
Figure 4. Surface microstructures of the (a)70BZT-30BCT, (b)60BZT-40BCT, (c)50BZT-50BCT, and (d) 40BZT-60BCT ceramics sintered at 1450 °C for 3 hours, presenting the largest grain size was observed in the 50BZT-50BCT ceramic.

However, there are some peaks that are not fitted well. Also, the presence of weak left shoulder was unexpectedly observed in the SXPD profiles, especially for the $\{200\}_p$ reflection, as seen in Figure 3(c). These results may be attributed to the occurrence of various mixed phases observed in the (1-x)BZT-(x)BCT ceramics near phase convergence region, leading to the distortion of crystal lattice and consequently originated the observed weak left shoulder and the variation between calculated and experimental curves in the fit [20]. The employment of temperature-dependent XRD in combination to Extended X-ray Absorption Fine Structure (EXAFS) measurements can be conducted to clarify the origin of weak shoulder [21].

3.2 Microstructural observation

Figure 4 illustrates SEM micrographs of the (1-x)BZT-(x)BCT ceramics where x = 0.3 mol% to 0.6 mol% using SEM in secondary electron mode with accelerating voltage of 15 kV. It was found that changes of BCT content had a strong influence on the observed grain size. The abnormal grain growth with average grain size of 5.4 μm ± 0.9 μm was observed in the 70BZT-30BCT ceramic. When adding more BCT content, small increase in grain size occurred to 6.6 μm ± 1.1 μm for the 60BZT-40BCT ceramic and reached the maximum grain size of 11.1 μm ± 1.8 μm for the 50BZT-50BCT ceramic. This observation of grain size variation is consistent with the result reported by Acosta *et al.* [22] However, as BCT content increased further to 40BZT-60BCT ceramic, the average grain size slightly dropped to 8.1 μm ± 1.5 μm. Ene *et al.* observed that the presence of ferroelectric-paraelectric phase transition can be influenced by the variation of grain size [23]. Moreover, a terrace-type morphology was obviously observed in the 50BZT-50BCT ceramic, as indicated by an arrow in Figure 4(c). This is a consequence of the formation of abnormal grain growth during sintering at high temperature [24].

3.3 Dielectric properties

Dielectric properties of materials play a vital role for using as energy storage capacitors, microelectronic devices, and high-voltage insulations. The occurrence of polarization under alternating electric field with different frequency is strongly impacted on the observed dielectric permittivity (ε_r) [25]. In this work, the frequency-dependent dielectric permittivity (ε_r) and loss tangent (tan δ) behaviors for the (1-x)BZT-(x)BCT ceramics were evaluated between the frequency range of 10 Hz to 10^6 Hz at room temperature. Figure 5(a) shows that the highest frequency-dependent ε_r (~3214 at 10 Hz) was found in the composition of 70BZT-30BCT, while the 40BZT-60BCT ceramic presented the lowest ε_r (~1810 at 10 Hz). This is possibly attributed to the occurrence of T phase as BCT content increases, resulting in the enhancement of hardening effect and the decrease of reversible polarization [14]. In addition, it can be seen that the ε_r gradually decreased when increasing frequency from 10 Hz to 10^6 Hz in all compositions. This can be explained by the drop of polarization response under high-frequency alternating field [25]. In terms of tan δ, various factors, for instances, chemical composition, microstructure, temperature, frequency, etc. have an influence on tan δ [26]. This work found that the 50BZT-50BCT ceramic showed the largest tan δ in low frequency range, as seen in Figure 5(b), implying that the movement of domain wall strongly occurred in this composition [26].

3.4 Ferroelectric properties

Figure 6 illustrates the polarization-electric field (P-E) ferroelectric hysteresis loop of the (1-x)BZT-(x)BCT ceramics measured at room temperature with the comparison of saturation polarization (P_{sat}), remanent polarization (P_r), the difference between P_{sat} and P_r (ΔP), and coercive field (E_c) as a function of composition. The well-saturated P-E hysteresis loop was observed in all compositions with a slight difference between P_{sat}, P_r, ΔP, and E_c, indicating a nonlinear feature of ferroelectrics [27]. Although, the 70BZT-30BCT composition previously showed the highest ε_r, the lowest P_{sat}, P_r, and E_c of 14.30 μC·cm^{-2}, 2.80 μC·cm^{-2}, and 1.59 kV·cm^{-1}, respectively, were observed in this composition. Moreover, as further adding BCT contents, the P_{sat}, P_r, and E_c gradually enhanced and reached the highest values of 17.42 μC·cm^{-2}, 8.22 μC·cm^{-2}, and 6.12 kV·cm^{-1} in the 40BZT-60BCT composition. In contrast, a slight drop of ΔP was observed when increasing BCT content. This is contradict to the results obtained by Liu *et al.* that found the highest ε_r, P_{sat}, P_r with the lowest E_c in the 50BZT-50BCT [8]. There are several factors that may be affected by the presence of polarization and coercive field such as preparation conditions, measurement condiciton, thermal treatment, mechanical stress, the presence of charge defects, etc. [28]
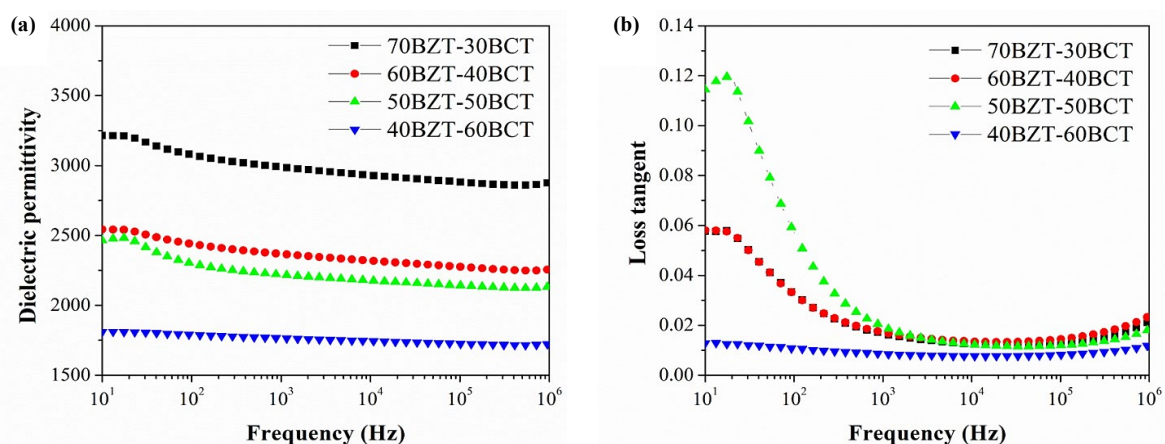
Figure 5. The frequency dependence of (a) dielectric permittivity and (b) loss tangent of the (1-x)BZT-(x)BCT ceramics measured at room temperature.
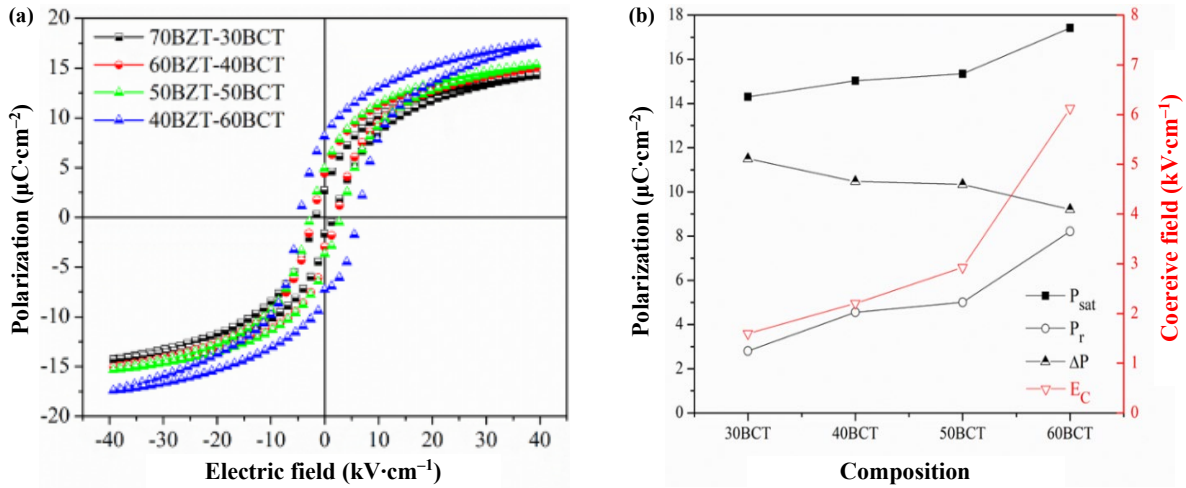
Figure 6. (a) The polarization-electric field hysteresis loops and (b) the comparison of saturation polarization, remanent polarization, and coercive field of the (1-x)BZT-(x)BCT ceramics measured at room temperature.

It is difficult to explain this result, but it might be related to the variation in irreversible and reversible polarizations when applying an electric field [29]. For dielectric properties shown previously in section 3.3, the response of reversible polarization were evaluated via the presence of ε_r, implying that the reversible polarization was strongly observed in the 70BZT-30BCT ceramic and consequently led to the observed highest ε_r. On the other side, the P-E hysteresis loop was employed to investigate both reversible and irreversible polarizations; the observed ΔP and P_r were attributed to the reversible and irreversible polarizations, respectively. In this work, the observed P_r slightly increased with increasing the BCT content, indicating that the enhancement of irreversible polarization was found. Moreover, the largest of ΔP was also observed in the 70BZT-30BCT ceramic, indicating that the highest of reversible polarization was observed, which consistent with the ε_r result. In addition, Acosta *et al.* reported that the hardening effect of the BZT-xBCT system became stronger when approaching the T phase, resulting in the highest quality factor (Q_m) was observed in the BZT-xBCT system where x = 0.6 [14]. This result is in good agreement with the P-E hysteresis loop of the 40BZT-60BCT ceramic in this work that found the O-T coexisting phases with 71% of T-phase fraction, as shown in Table 1. As a result, the increase in E_c and the decrease in ΔP were observed when increasing the BCT content, as seen in Figure 6(b).

3.5 Energy storage properties

The stored energy density (W_{st}), the recoverable energy (W_{rec}), energy loss (W_{loss}), and energy conversion efficiency (η) are key parameters for evaluating energy storage properties by dynamic method [30]. For ferroelectric material like the (1-x)BZT-(x)BCT ceramic, when charging by applying electric field to the maximum value (E_{max}), the maximum polarization (P_{max}) is obtained and the W_{st} can be estimated by Equation (1).

$$W_{st} = \int_0^{P_{max}} E \, dP \qquad (1)$$

During discharging, the W_{loss} occurs, resulting in the presence of the W_{rec} which related to the area above the discharging curve from P_{max} to P_r. Hence, the W_{rec} and η can be calculated by Equation (2) and Equation (3), respectively [31].

$$W_{rec} = \int_{P_r}^{P_{max}} E \, dP \qquad (2)$$

$$\eta \ (\%) = \frac{W_{rec}}{W_{rec} + W_{loss}} \times 100 \qquad (3)$$

Figure 7 shows the variation of field-induced energy conversion efficiency (η) for the (1-x)BZT-(x)BCT ceramics near phase convergence region evaluated from the P-E hysteresis loop under the application of electric field between 10 and 40 kV·cm^{-1}. It was found that the W_{rec} and W_{loss} increased with increasing the electric field, leading to the enhancement of η was observed in all compositions. Moreover, the 70BZT-30BCT composition that found the coexistence of R-C phases presented the highest η of 70.4% at 40 kV·cm^{-1}, while the lowest η of 45.1% was observed in the 40BZT-60BCT composition that showed the T-C coexisting phases. This is possibly attributed to the occurrence of softening and hardening behaviors, leading to the variation in the E_c and ΔP that could impact on the observed η in the (1-x)BZT-(x)BCT ceramics. As described earlier in section 3.4, the hardening effect and irreversible polarization were strongly observed in the 40BZT-60BCT ceramic due to the occurrence of T phase. Consequently, the largest amount of E_c and P_r with the lowest ΔP were found, resulting in the presence of the smallest η. On the other side, it was explained that R phase could affect the presence of softening behavior [14]. Therefore, the improvement of ΔP was found when reducing BCT content and approaching to R phase, leading to the highest η was observed in the 70BZT-30BCT ceramic. Sya *et al.* reported a high efficiency η of 72.1% that observed in the BZT-40BCT ceramic prepared by sol-gel method [32]. Moreover, Maier *et al.* found that the improvement of energy storage performance could be obtained by the application of stress [33].
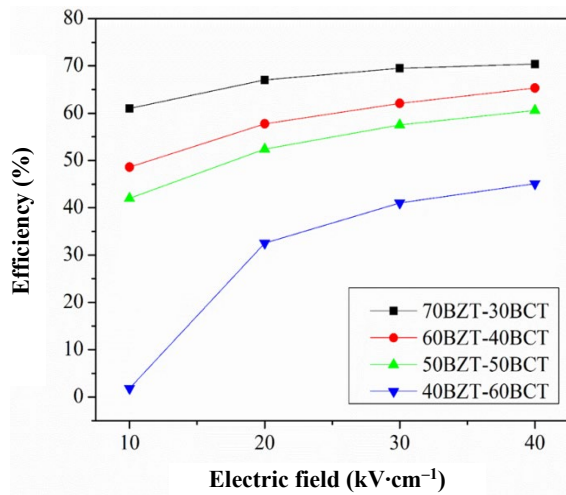
Figure 7. Energy conversion efficiency of the (1-x)BZT-(x)BCT ceramics as a function of electric field from 10 to 40 kV·cm^{-1}, indicating that the maximum efficiency was observed in the 70BZT-30BCT ceramic.

3.6 Piezoelectric properties

Figure 8 illustrates the composition-driven electromechanical behavior of the (1-x)BZT-(x)BCT ceramics near the phase convergence region. Interestingly, Figure 8(a) showed that the average maximum strain of 0.16% was observed in the 50BZT-50BCT composition, although the highest εr and Psat were not obtained in this composition. In contrast to several publications on the (1-x)BZT-(x)BCT ceramics, the composition that showed the largest polarization was also observed the highest dielectric permittivity and piezoelectric properties [8,11,34]. This contradiction suggests that the presence of piezoelectric activity in the (1-x)BZT-(x)BCT system is not only dependent on the polarization response. The extrinsic contribution from non-180° domain switching is significantly attributed to the occurrence of strain (greater than 50% of the total output) under the applied field. Moreover, the domain size, morphology, mobility and activation barrier can influence on the domain-switching behavior [22].
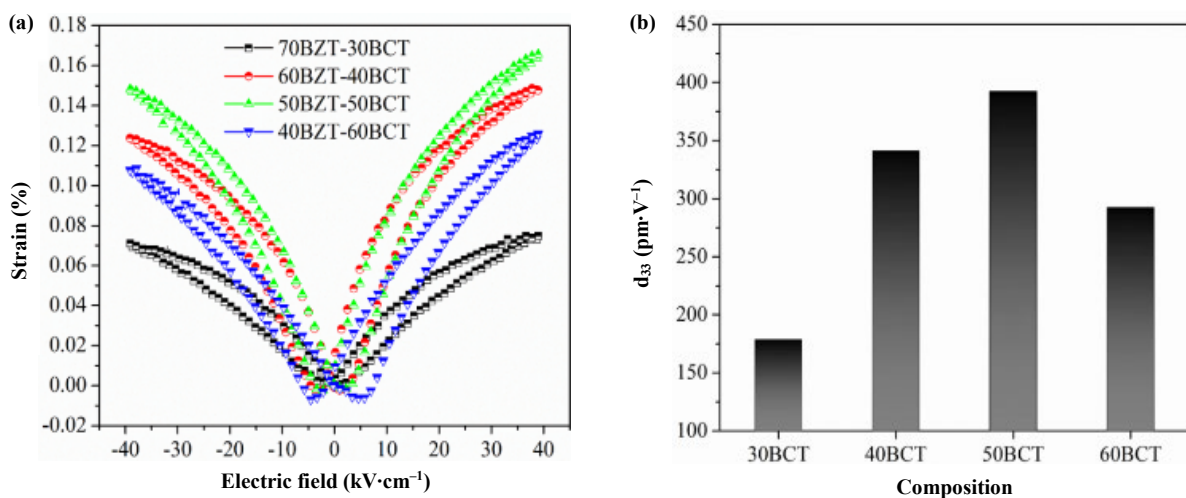
In addition, the converse piezoelectric coefficient (d33) for each composition was determined using the maximum strain divided by the applied field [35]. It was found that the lowest d33 of 179 pm·V^{-1} was observed in the 70BZT-30BCT ceramic, see in Figure 8(b). As the BCT content increased, the coexistence of ferroelectric-ferroelectric phases was observed in the 60BZT-40BCT (R-O coexisting phases) and 50BZT-50BCT (O-T coexisting phases), resulting in the enhancement of d33 was found with the maximum d33 of 393 pm·V^{-1} observed in the 50BZT-50BCT composition. When further increased the BCT content to 60BCT, a gradual drop of d33 to 293 pm·V^{-1} was obtained because of the occurrence of paraelectric C phase, as shown in Table 1. A possible explanation for the observed highest d33 in the 50BZT-50BCT composition in this work may be attributed to the observed largest grain size that can enhance the movement of domain wall [36]. However, the nature of R-O and O-T mixed phases is still unclear and needs further investigations to clarify why the coexistence of O-T exhibits d33 higher than the R-O mixed phases [22].

4. Conclusions

The structure-property relationships of the (1-x)BZT-(x)BCT ceramics where x = 0.3-0.6 mol% were investigated via high-resolution synchrotron x-ray diffraction in this work. It was found that changes of coexisting phases had a strong impact on the observed functional properties. Moreover, the distortion of crystal lattice due to the occurrence of mixed phases could impact on the presence of weak left shoulder in the SXPD profiles. In addition, the highest εr was observed in the 70BZT-30BCT composition near the phase convergence region, while the 40BZT-60BCT composition near the O-T phase boundary showed the largest Psat and Pr. However, the coexistence of O-T phases that observed in the 50BZT-50BCT composition had a significant influence on the presence of maximum strain and d33 piezoelectric coefficient. It was suggested that the functional properties of the (1-x)BZT-(x)BCT ceramics are not dependent on the reversible and irreversible polarizations under the application of electric field. The contribution of non-180° domain switching also plays a vital role, especially in the piezoelectric properties.

Figure 8 (a) The strain-electric field butterfly loop and (b) the converse d$_{33}$ piezoelectric coefficient measured at room temperature of the (1-x)BZT-(x)BCT ceramics, indicating that the highest d$_{33}$ was obsevred in the 50BZT-50BCT ceramic.

Acknowledgements

References

[1]   G. Wang, Z. Lu, Y. Li, L. Li, H. Ji, A. Feteira, D. Zhou, D. Wang, S. Zhang, and I. Reaney, "Electroceramics for high-energy density capacitors: Current status and future perspectives," *Chemical Reviews,* vol. 121, no. 10, pp. 6124-6172, 2021.

[2]   P. S. Kadhane, B. G. Baraskar, T. C. Darvade, A. R. James, and R. C. Kambale, "Ferroelectric and piezoelectric properties of Ca^{2+} and Sn^{4+} substituted $BaTiO_3$ lead-free electroceramics on the emphasis of phase coexistence," *Solid State Communications,* vol. 306, p. 113797, 2020.

[3]   J. Rödel, W. Jo, K. T. P. Seifert, E.-M. Anton, T. Granzow, and D. Damjanovic, "Perspective on the Development of Lead-free Piezoceramics," *Journal of the American Ceramic Society,* vol. 92, no. 6, pp. 1153-1177, 2009.

[4]   C.-H. Hong, H.-P. Kim, B.-Y. Choi, H.-S. Han, J. S. Son, C. W. Ahn, and W. Jo, "Lead-free piezoceramics – Where to move on?," *Journal of Materiomics,* vol. 2, no. 1, pp. 1-24, 2016.

[5]   M. Acosta, N. Novak, V. Rojas, S. Patel, R. Vaish, J. Koruza, G. A. Jr. Rossetti, and J. Rödel, "$BaTiO_3$-based piezoelectrics: Fundamentals, current status, and perspectives," *Applied Physics Reviews,* vol. 4, no. 4, p. 041305, 2017.

[6]   M. Maraj, W. Wei, B. Peng, and W. Sun, "Dielectric and energy storage properties of $Ba_{(1-x)}Ca_xZr_yTi_{(1-y)}O_3$ (BCZT): A review," *Materials*, vol. 12, no. 21. 2019.

[7]   J. Rödel, and J.-F. Li, "Lead-free piezoceramics: Status and perspectives," *MRS Bulletin,* vol. 43, no. 8, pp. 576-580, 2018.

[8]   W. Liu, and X. Ren, "Large piezoelectric effect in Pb-free ceramics," *Physical Review Letters,* vol. 103, no. 25, p. 257602, 2009.

[9]   D. S. Keeble, F. Benabdallah, P. A. Thomas, M. Maglione, and J. Kreisel, "Revised structural phase diagram of $(Ba_{0.7}Ca_{0.3}TiO_3)$-$(BaZr_{0.2}Ti_{0.8}O_3)$," *Applied Physics Letters,* vol. 102, no. 9, p. 092903, 2013.

[10] J. Gao, X. Ke, M. Acosta, J. Glaum, and X. Ren, "High piezo-electricity by multiphase coexisting point: Barium titanate derivatives," *MRS Bulletin,* vol. 43, no. 8, pp. 595-599, 2018.

[11] L. Zhang, M. Zhang, L. Wang, C. Zhou, Z. Zhang, Y. Yao, L. Zhang, D. Xue, X. Lou, and X. Ren, "Phase transitions and the piezoelectricity around morphotropic phase boundary in $Ba(Zr_{0.2}Ti_{0.8})O_3$-x$(Ba_{0.7}Ca_{0.3})TiO_3$ lead-free solid solution," *Applied Physics Letters,* vol. 105, no. 16, p. 162908, 2014.

[12] Y. Tian, L. Wei, X. Chao, Z. Liu, and Z. Yang, "Phase transition behavior and large piezoelectricity near the morphotropic phase boundary of lead-free $(Ba_{0.85}Ca_{0.15})(Zr_{0.1}Ti_{0.9})O_3$ ceramics,"

Journal of the American Ceramic Society, vol. 96, no. 2, pp. 496-502, 2013.

[13] M. C. Ehmke, J. Glaum, M. Hoffman, J. E. Blendell, and K. J. Bowman, "The effect of electric poling on the performance of lead-free (1−x)$Ba(Zr_{0.2}Ti_{0.8})O_3$–x$(Ba_{0.7}Ca_{0.3})TiO_3$ piezoceramics," *Journal of the American Ceramic Society,* vol. 96, no. 12, pp. 3805-3811, 2013.

[14] M. Acosta, N. Khakpash, T. Someya, N. Novak, W. Jo, H. Nagata, G.A. Rossetti, and J. Rödel, "Origin of the large piezoelectric activity in (1−x)$Ba(Zr_{0.2}Ti_{0.8})O_3$-x$(Ba_{0.7}Ca_{0.3})TiO_3$ ceramics," *Physical Review B,* vol. 91, no. 10, p. 104108, 2015.

[15] S. Gražulis, D. Chateigner, R.T. Downs, A.F. Yokochi, M. Quirós, L. Lutterotti, E. Manakova, J. Butkus, P. Moeck, A. Le Bail, "Crystallography open database - an open-access collection of crystal structures,", *Journal of applied crystallography,* vol. 42, no. Pt 4, pp. 726-729, 2009.

[16] M. I. Mendelson, "Average grain size in polycrystalline ceramics," *Journal of the American Ceramic Society,* vol. 52, no. 8, pp. 443-446, 1969.

[17] A. Bjørnetun Haugen, J. S. Forrester, D. Damjanovic, B. Li, K. J. Bowman, and J. L. Jones, "Structure and phase transitions in 0.5$(Ba_{0.7}Ca_{0.3}TiO_3)$-0.5$(BaZr_{0.2}Ti_{0.8}O_3)$ from −100°C to 150°C," *Journal of Applied Physics,* vol. 113, no. 1, p. 014103, 2013.

[18] M. Gao, W. Ge, X. Li, H. Yuan, C. Liu, H. Zhao, Y. Ma, Y. Chang, "Enhanced dielectric and energy storage properties in Fe-doped BCZT ferroelectric ceramics," P*hysica status solidi (a),* vol. 217, no. 16, p. 2000253, 2020.

[19] W. Li, Z. Xu, R. Chu, P. Fu, and G. Zang, "Structural and dielectric properties in the $(Ba_{1-x}Ca_x)(Ti_{0.95}Zr_{0.05})O_3$ ceramics," *Current Applied Physics,* vol. 12, no. 3, pp. 748-751, 2012.

[20] J. Kondoh, "Origin of the hump on the left shoulder of the X-ray diffraction peaks observed in Y_2O_3-fully and partially stabilized ZrO_2," *Journal of Alloys and Compounds,* vol. 375, no. 1, pp. 270-282, 2004.

[21] J. Kondoh, T. Kawashima, S. Kikuchi, Y. Tomii, and Y. Ito, "Effect of aging on yttria-stabilized zirconia: I. A study of its electrochemical properties," *Journal of The Electrochemical Society,* vol. 145, no. 5, pp. 1527, 1998.

[22] M. Acosta, N. Novak, W. Jo, and J. Rödel, "Relationship between electromechanical properties and phase diagram in the $Ba(Zr_{0.2}Ti_{0.8})O_3$–x$(Ba_{0.7}Ca_{0.3})TiO_3$ lead-free piezoceramic," *Acta Materialia,* vol. 80, pp. 48-55, 2014.

[23] V. L. Ene, V.R. Lupu, C.V. Condor, R.E. Patru, L.M. Hrib, L. Amarande, A.I. Nicoara, L. Pintilie, and A.C. Ianculescu, "Influence of grain size on dielectric behavior in lead-free 0.5 $Ba(Zr_{0.2}Ti_{0.8})$ O_3-0.5$(Ba_{0.7}Ca_{0.3})TiO_3$ ceramics," *Nanomaterials,* vol. 13, no. 22, 2023.

[24] G. Herrera-Pérez, I. Castillo-Sandoval, O. Solís-Canto, G. Tapia-Padilla, A. Reyes-Rojas, and L. E. Fuentes-Cobas, "Local piezo-response for lead-free $Ba_{0.9}Ca_{0.1}Ti_{0.9}Zr_{0.1}O_3$ electro-ceramic by switching spectroscopy," *Materials Research,* vol. 21, 2018.

[25] L. Chen, C. Kim, R. Batra, J.P. Lightstone, C. Wu, Z. Li, A.A. Deshmukh, Y. Wang, H.D. Tran, P. Vashishta, G.A. Sotzing, Y. Cao, and R. Ramprasad, "Frequency-dependent dielectric constant prediction of polymers using machine learning," *Computational Materials,* vol. 6, no. 1, p. 61, 2020.

[26] K. H. Härdtl, "Electrical and mechanical losses in ferroelectric ceramics," *Ceramics International,* vol. 8, no. 4, pp. 121-127, 1982.

[27] Y. B. Adediji, A. M. Adeyinka, D. I. Yahya, and O. V. Mbelu, "A review of energy storage applications of lead-free $BaTiO_3$-based dielectric ceramic capacitors," *Energy, Ecology and Environment,* vol. 8, no. 5, pp. 401-419, 2023.

[28] D. Dragan, "Ferroelectric, dielectric and piezoelectric properties of ferroelectric thin films and ceramics," *Reports on Progress in Physics,* vol. 61, no. 9, p. 1267, 1998.

[29] J. Gao, X. Hu, Y. Wang, Y. Liu, L. Zhang, X. Ke, L. Zhong, H. Zhao, and X. Ren, "Understanding the mechanism of large dielectric response in Pb-free $(1-x)Ba(Zr_{0.2}Ti_{0.8})O_3-x(Ba_{0.7}Ca_{0.3})TiO_3$ ferroelectric ceramics," *Acta Materialia,* vol. 125, pp. 177-186, 2017.

[30] A. R. Jayakrishnan, J. P. B. Silva, K. Kamakshi, D. Dastan, V. Annapureddy, M. Pereira, and K. C. Sekhar, "Are lead-free relaxor ferroelectric materials the most promising candidates for energy storage capacitors?," *Progress in Materials Science,* vol. 132, 2023.

[31] Z. Hanani, S. Merselmiz, M. Amjoud, D. Mezzane, M. Lahcini, J. Ghanbaja, M. Spreitzer, D. Vengust, M. El Marssi, I.A. Luk'yanchuk, Z. Kutnjak, B. Rožič, and M. Gouné, "Novel lead-free BCZT-based ceramic with thermally-stable recovered energy density and increased energy storage efficiency," *Journal of Materiomics,* vol. 8, no. 4, pp. 873-881, 2022.

[32] R. Syal, P. Sharma, S. Singh, and S. Kumar, "Investigation of energy storage properties in lead-free BZT-40BCT relaxor ceramic," *Materials Today: Proceedings,* 2023.

[33] J. G. Maier, A. Gadelmawla, N. H. Khansur, and K. G. Webber, "Stress-induced tailoring of energy storage properties in lead-free $Ba_{0.85}Ca_{0.15}Zr_{0.1}Ti_{0.9}O_3$ ferroelectric bulk ceramics," *Journal of Materiomics,* vol. 9, no. 4, pp. 673-682, 2023.

[34] M. B. Abdessalem, S. Aydi, A. Aydi, N. Abdelmoula, Z. Sassi, and H. Khemakhem, "Polymorphic phase transition and morphotropic phase boundary in $Ba_{1-x}Ca_xTi_{1-y}Zr_yO_3$ ceramics," *Applied Physics A,* vol. 123, no. 9, 2017.

[35] N. Boothrawong, L. Tawee, S. Thammarong, P. Jaita, D. R. Sweatman, G. Rujijanagul, and T. Tunkasiri, "Dependence of applied electric fields on electrical properties of BCZT ceramic," *ScienceAsia,* vol. 49, no. 3, pp. 344-352, 2023.

[36] S. Merselmiz, Z. Hanani, D. Mezzane, A.G. Razumnaya, M. Amjoud, L. Hajji, S. Terenchuk, B. Rozic, I.A. Luk'yanchuk, and Z. Kutnjak, "Thermal-stability of the enhanced piezoelectric, energy storage and electrocaloric properties of a lead-free BCZT ceramic," *RSC Adv,* vol. 11, no. 16, pp. 9459-9468, 2021.